Biological Psychiatry

Archival Report

Dynamically Timed Stimulation of Corticolimbic Circuitry Activates a Stress-Compensatory Pathway

David Carlson, Lisa K. David, Neil M. Gallagher, Mai-Anh T. Vu, Matthew Shirley, Rainbo Hultman, Joyce Wang, Caley Burrus, Colleen A. McClung, Sunil Kumar, Lawrence Carin, Stephen D. Mague, and Kafui Dzirasa

ABSTRACT

BACKGROUND: The prefrontal cortex plays a critical role in regulating emotional behaviors, and dysfunction of prefrontal cortex–dependent networks has been broadly implicated in mediating stress-induced behavioral disorders including major depressive disorder.

METHODS: Here we acquired multicircuit in vivo activity from eight cortical and limbic brain regions as mice were subjected to the tail suspension test (TST) and an open field test. We used a linear decoder to determine whether cellular responses across each of the cortical and limbic areas signal movement during the TST and open field test. We then performed repeat behavioral testing to identify which brain areas show cellular adaptations that signal the increase in immobility induced by repeat TST exposure.

RESULTS: The increase in immobility observed during repeat TST exposure is linked to a selective functional upregulation of cellular activity in infralimbic cortex and medial dorsal thalamus, and to an increase in the spatiotemporal dynamic interaction between these structures. Inducing this spatiotemporal dynamic using closed-loop optogenetic stimulation is sufficient to increase movement in the TST in stress-naive mice, while stimulating above the carrier frequency of this circuit suppressed movement. This demonstrates that the adaptations in infralimbic cortex–medial dorsal thalamus circuitry observed after stress reflect a compensatory mechanism whereby the brain drives neural systems to counterbalance stress effects.

CONCLUSIONS: Our findings provide evidence that targeting endogenous spatiotemporal dynamics is a potential therapeutic approach for treating stress-induced behavioral disorders, and that dynamics are a critical axis of manipulation for causal optogenetic studies.

Keywords: Depression, Infralimbic cortex, Limbic, Neural network, Synchrony, Thalamus

http://dx.doi.org/10.1016/j.biopsych.2017.06.008

Major depressive disorder (MDD) is the leading cause of disability in the world. Despite the heterogeneous nature of the disorder, multiple studies support hyperactivity and/or network hyperconnectivity involving the subgenual cingulate cortex (Brodmann area 25) as key neurophysiological alterations in MDD (1–3). Though these neural biomarkers have been exploited to guide the development of deep brain stimulation and transcranial magnetic stimulation into viable MDD therapeutics (4,5), we hypothesize that the spatiotemporal dynamics are a key feature associated with subgenual cingulate cortex–dependent network pathology in MDD. Knowledge of these pathological dynamics would be particularly important because they potentially could be controlled to optimize brain stimulation–based therapies.

In this study, we used a data-driven strategy to identify the brain regions in mice that showed neural processing adaptations in response to repeat tail suspension stress. Using machine learning, we found that repeat tail suspension stress induced hyperreactivity in the infralimbic cortex (IL), which is the rodent anatomical equivalent of the subgenual cingulate cortex in humans based on anatomical connections (6). We then developed a closed-loop stimulation system based on the precise spatiotemporal alterations observed in IL-dependent long-range circuitry after stress exposure. In particular, we monitored the activity within the circuit and controlled activity in medial dorsal thalamus (Thal) in a way that produced a specific set of spatiotemporal dynamics within the whole circuit. Closed-loop stimulation increased tail suspension test (TST) activity in stress-naive mice, while two standard fixed-frequency stimulation patterns either failed to show effects or suppressed movement. We suggest that spatiotemporal dynamics that are endogenously activated in healthy animals to compensate for stress pathology can by harnessed and exploited to optimize brain stimulation–based treatments.

ISSN: 0006-3223

The TST is a classic assay used to probe the impact of antidepressant therapeutics on the behavioral response of mice to a challenging experience (7,8). In this assay, mice are subjected to an inescapable stressor in which they are suspended upside down by their tail. The test induces a robust stress response (9), and the time animals spend immobile relative to the time they spend engaging in escape actions is interpreted as an indicator of their behavioral response to the uncontrollable stressor (7). Critically, prior exposure to stress diminishes behavioral responses during the TST (10). Thus, the TST assays an animal's behavioral adaptation in response to prior stress exposure, and the test in and of itself induces a strong stress response. We exploited these two features of the test for our experiments. First, we measured behavioral and neurophysiological activity continuously during the TST (Figure 1A). We defined the strength of the neural responses during an initial TST session in naive mice. We then repeated testing on the subsequent day. This approach diminished their behavioral responses on the TST. Overall, this experimental strategy allowed us to monitor neural responses in the same animals when they were stress naive, and again after exposure to stress (in this case, the stress induced by the first TST session) using a single behavioral assay that is responsive to stress. We then uncovered the spatiotemporal dynamics across the specific brain areas that showed neural adaptions during the repeat test. Finally, we also performed control behavioral experiments using repeating testing in an open field.

METHODS AND MATERIALS

Animal Care and Use

Clock-Δ19 mice were created by *N*-ethyl-*N*-nitrosurea mutagenesis and produce a dominant-negative circadian locomoter output cycles kaput protein as previously described (11). Mice used for TST recording experiments were bred from heterozygous ($Clock^{\Delta 19}/+$) mice that were backcrossed >8 generations onto a BALB/CJ strain background. The breeders were initially maintained on a BALB/CJ and C57BL/6J mixed strain background before backcrossing. Male *Clock*-Δ19 ($Clock^{\Delta 19}/Clock^{\Delta 19}$) and wild-type (+/+) littermate control mice were used for all electrophysiological recording experiments presented in this study. Inbred BALB/cJ male mice (strain: 000651) purchased from the Jackson Laboratory (Bar Harbor, ME) were used for optogenetic stimulation and neural Closed Loop Actuator for Synchronization Phase (*nCLASP*) experiments. Mice were housed 3 to 5 per cage on a 12-hour light/dark cycle, and maintained in a humidity- and temperature-controlled room with water and food available ad libitum. Behavioral and electrophysiological experiments were conducted during the light cycle (Zeitgeber time 4–12). All studies were conducted with approved protocols from the Duke University Institutional Animal Care and Use Committees and were in accordance with the National Institutes of Health guidelines for the Care and Use of Laboratory Animals.

Behavioral Testing

Headstages were connected without anesthesia, and animals were habituated to the recording room for 90 minutes prior to testing. All behavioral testing was conducted under low-illumination conditions (1–2 lx). Mice were initially placed in a 17.5-inch-long × 17.5-inch-wide × 11.75-inch-high chamber for 5 minutes of open field testing (OFT). The location of the animals was acquired in real time using NeuroMotive (Blackrock Microsystems, Inc., Salt Lake City, UT). Mice were then transferred to a TST apparatus (MED-TSS-MS; Med Associates, Inc., St. Albans, VT) that was modified to allow for continuous acquisition of animal motion. Mice were suspended 1 cm from the tip of their tail for 10 minutes. The activity trace was digitized at 2000 Hz and stored in real time with our neurophysiological recording data. OFT and TST neurophysiological data were acquired during a single testing session, and the behavior testing session was repeated the next day. The quality of video tracking was confirmed offline using NeuroMotive.

Neurophysiological Data Acquisition

Neurophysiological recordings were performed during the OFT and TST. Neuronal activity was sampled at 30 kHz, high-pass filtered at 500 Hz, sorted online, and stored using the CerePlex Direct acquisition system (Blackrock Microsystems, Inc.). Neuronal data were referenced online against a wire within the same brain area that did not exhibit a signal-to-noise ratio greater than 3:1. At the end of the recording, cells were sorted again using an offline sorting algorithm (Plexon Inc., Dallas, TX) to confirm the quality of the recorded cells. Local field potentials (LFPs) were bandpass filtered at 0.5 to 250 Hz and stored at 1000 Hz. All neurophysiological recordings were referenced to a ground wire connected to both ground screws. Video recordings were acquired in real time using NeuroMotive and synchronized with neurophysiological data.

RESULTS

Broad cortical and limbic firing signaled TST-related behavior during the initial TST session. We used an unbiased approach to perform in vivo neurophysiological recordings of action potentials and LFPs. Specifically, animals were implanted in the IL and seven additional brain regions that mediate emotional behavior, including the prelimbic cortex, nucleus accumbens (core and shell), amygdala (AMY) (basolateral AMY and central AMY), Thal, dorsal hippocampus, and ventral tegmental area. Recordings were obtained while animals were subjected to a TST, and each recording session was immediately preceded by an OFT run in low lighting conditions so as to be nonstressful. This enabled us to distinguish movement-related neuronal responses in the TST from those responses observed in a nonstressful test (Figure 1A). The location of each mouse was recorded continuously during the OFT using video tracking, and behavioral activity was measured continuously during the TST using an accelerometer. When we performed event triggered averaging analysis relative to movement onset/offset, we found a wide array of neural responses. For example, we found cells that fired with movement onset, cells that fired prior to movement, and cells that fired after movement was initiated (see Figure 1B; see also Supplemental Figure S1 for examples). To quantify the relationship between cellular firing and the complex patterns of movements measured during the two behavioral tests, we

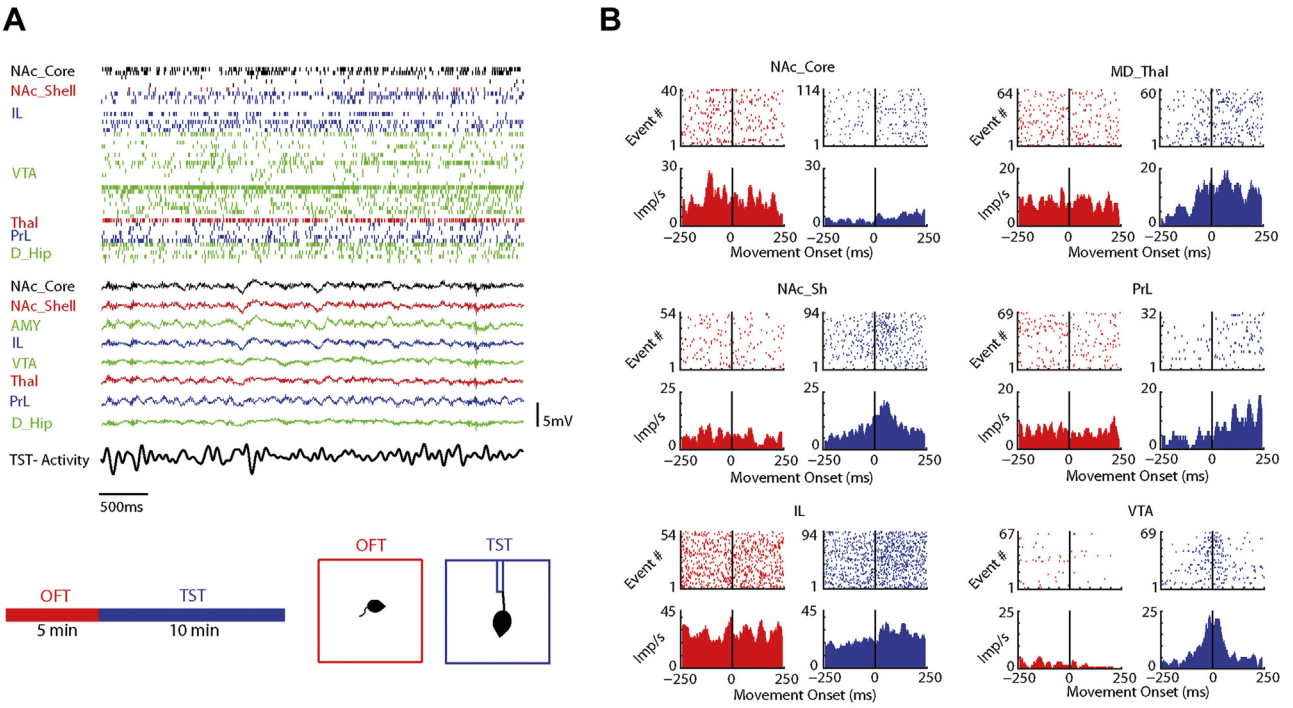
A
NAc_Core
NAc_Shell
IL
VTA
Thal
PrL
D_Hip
5mV
TST- Activity
500ms
OFT
TST
5 min
10 min
B
NAc_Core
MD_Thal
NAc_Sh
PrL
IL
VTA
Event #
Imp/s
Movement Onset (ms)

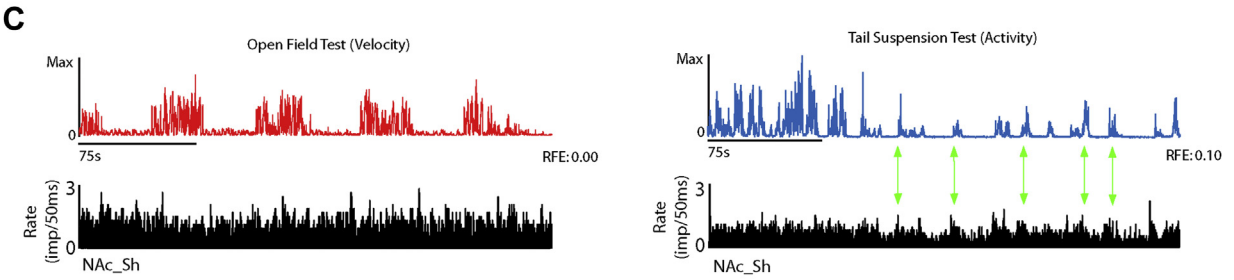
C
Open Field Test (Velocity)
Max
75s
RFE: 0.00
Rate (imp/50ms)
NAc_Sh
Tail Suspension Test (Activity)
RFE: 0.10

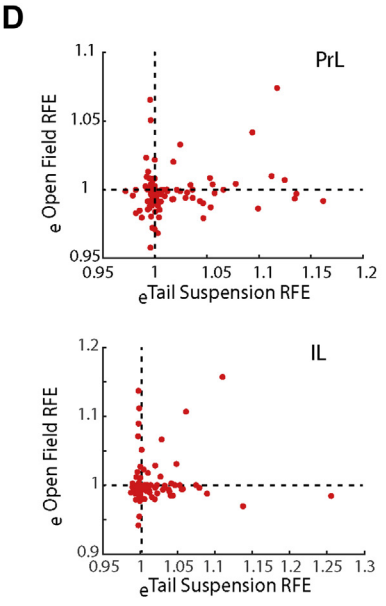
D
PrL
IL
e Open Field RFE
eTail Suspension RFE

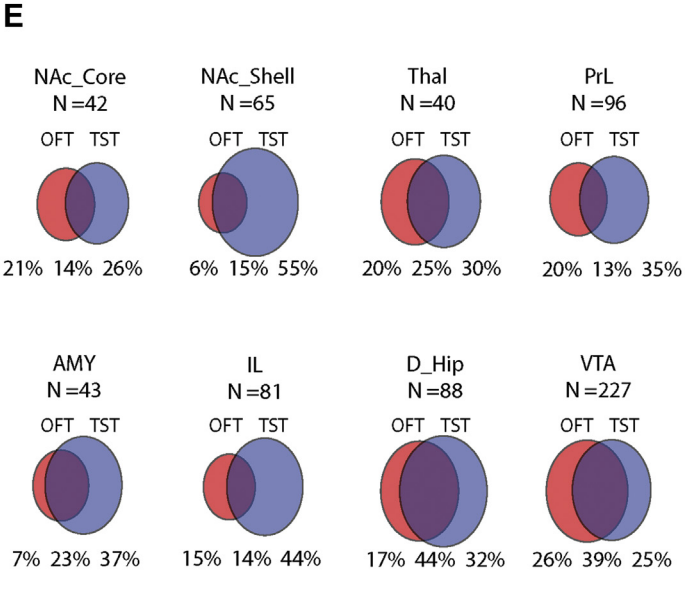
E
NAc_Core N =42
NAc_Shell N =65
Thal N =40
PrL N =96
AMY N =43
IL N =81
D_Hip N =88
VTA N =227
OFT TST
21% 14% 26%
6% 15% 55%
20% 25% 30%
20% 13% 35%
7% 23% 37%
15% 14% 44%
17% 44% 32%
26% 39% 25%

employed a linear decoder. This decoder allowed us to model the extent to which any specific pattern of behavior observed during a task condition (e.g., movement onset, acceleration, velocity, deceleration, immobility) was related to the spiking of each neuron. This approach quantified movement relative to neuronal spiking (rather than neuronal spiking relative to movement [Figure 1B]; see also Supplemental Figure S4), by creating a model based on the behavioral profile observed in the 1-second window surrounding neuronal firing. This model returned an error metric, based on the reduction in fractional error (RFE) (12), that indicated how much behavioral variance was explained by the spiking of each neuron (Figure 1C). If any type of movement observed during a test condition was related to the firing of a neuron, the model returned an RFE value >0 (Figure 1D). On the other hand, if neuronal firing was not related to any type of movement observed during a test condition, the RFE returned a value ≤ 0. Using the decoder, we identified neurons from each cortical and limbic brain area that signaled movement during the TST, OFT, or both tests during the initial session (Figure 1D). Several areas, including the ventral tegmental area and dorsal hippocampus, showed neurons that encoded movement generated during both tests. Other areas, including the IL, the nucleus accumbens shell, and AMY, showed stronger bias toward signaling TST movement compared with movement in the OFT (Figure 1E). Thus as expected, because the OFT and TST are very different contexts, many neurons exhibited firing that was related to the specific patterns of movement elicited during each test condition (8,13).

Strikingly, when we trained additional linear decoders on data acquired during the TST session on the second day and compared them to the first TST session, we found that the brain-wide population of neurons showed an increase in their ability to signal TST movement, as evidenced by an overall increase in the RFE values obtained for the neurons' models (Kolmogorov-Smirnov test [$K_{stat} = 0.11$, $p < .001$]; $n = 647$ and 620 neurons during sessions 1 and 2, respectively; Figure 2A). As expected, animals exhibited higher immobility during the second testing session as well (paired t test [$t_{13} = 3.8$, $p = .002$]; $n = 14$; Figure 2C, left). In contrast, no differences were observed in open field movement-related signaling (Kolmogorov-Smirnov test [$K_{stat} = 0.06$, $p = .23$]; Figure 2B) or in the distance traveled in the open field between sessions (paired t test [$t_{13} = 0.3$, $p = .74$]; Figure 2C, right). Thus, both the neural and behavioral adaptations that occurred with repeat testing were specific to the stressful assay.

After finding that repeat exposure to the TST increased test-specific movement-related neuronal responses, we tested whether these neural changes were specific to any brain regions. We found that only the IL and Thal showed significant increases in the portion of TST-responsive neurons that showed an RFE >0 ($p < .05$ using G-test with Williams correction; Figure 2E). Thus, our unbiased approach suggested that the changes in behavior that occurred with repeat testing were selectively associated with changes in IL and Thal population activity. This increase in the portion of TST-responsive neurons suggested that either new IL-Thal neurons were added to the ensemble that encoded the TST movements observed during the first session, and/or that additional IL-Thal neurons signaled a new type of TST movement that emerged during the second session.

To determine whether the IL and Thal hyperreactivity observed in normal animals during the second TST session were behaviorally relevant and not simply a reflection of repeated exposure to the same TST assay, we performed our recording protocol in a genetic mouse line (*Clock*-Δ19 mice) that we have previously shown to exhibit resilience to multiple distinct assays of behavioral challenge including the forced swim test and learned helplessness (14–16). As expected, *Clock-Δ19* mice were resilient to the adaptation induced by repeated TST exposure in the full group of normal animals (for session $\times$ genotype interaction using two-way analysis of variance [ANOVA] [$F_{1,25} = 6.51$, $p = .017$]; for post hoc testing using a paired t test within *Clock-Δ19* genotype [$t_{12} = 0.2$, $p = .83$]; see Figure 2D). No differences in TST immobility were observed across genotype within the first testing session (post hoc testing across genotype using unpaired t test [$t_{25} = 0.3$, $p = .75$]). Thus, *Clock-Δ19* mice were resilient to the behavioral adaptation induced by repeat TST exposure. Critically, no changes in IL or Thal TST activity (or any of the other brain areas) were observed in the *Clock*-Δ19 mice (Figure 2F). Thus, repeat TST testing failed to induce IL or Thal hyperreactivity in a mouse model of stress resilience. This suggests that the reorganization of the IL and Thal that occurred with repeat TST was linked to the susceptibility of the wild-type animals to the initial exposure.

After determining that only the IL and Thal showed changes in TST-related firing during repeat testing, we set out to test whether repeat testing also altered neurophysiological interactions between these structures. Cross-frequency phase coupling (CFPC) analysis has been shown to signal emotional responses across corticolimbic circuitry (17,18). Thus, we calculated CFPC between the IL and Thal LFP activity. We limited our analysis to LFP segments selected from intervals when animals were immobile on the TST to ensure that difference in coupling observed across testing sessions did not simply reflect differences in the total movement (19). Using this approach, we found that the phase of 3-Hz to 7-Hz activity in IL coupled to the amplitude of low-gamma activity (30–70 Hz)

Figure 1. Distributed corticolimbic neuronal activity signals escape actions. **(A)** Raster plot showing unit and local field potential activity acquired concurrently from cortical and limbic brain areas during the tail suspension test (TST) (top). Schematic of behavioral recording sessions (bottom). **(B)** Raster plot and perievent time histograms showing examples of neuronal firing time locked to movement onset in the open field test (OFT) (red) and TST (blue). Histograms show average unit impulses per millisecond (imp/ms). **(C)** Example of firing rate histogram of a nucleus accumbens shell (NAc_Shell and NAc_Sh) neuron (bottom) relative to the movement activity trace (top) in the OFT (left) and TST (right). Note that for this neuron, high TST movement was observed during periods of high cell activity (green arrows highlight peak-to-peak correlations). **(D)** Example plots showing the relationship between spiking and behavioral activity for each of the prelimbic cortex (PrL) and infralimbic cortex (IL) neuron measured using a metric based on the reduction in fractional error (RFE). Units that showed e^{RFE} values >1 (RFE >0) explained signal action during each behavioral test. **(E)** Venn diagrams quantify the portion of neurons in each brain area that signal action during each behavioral test. All data shown is from wild-type mice. AMY, amygdala; D_Hip, dorsal hippocampus; MC_Thal, medial dorsal thalamus; NAc_Core, nucleus accumbens core; VTA, ventral tegmental area.

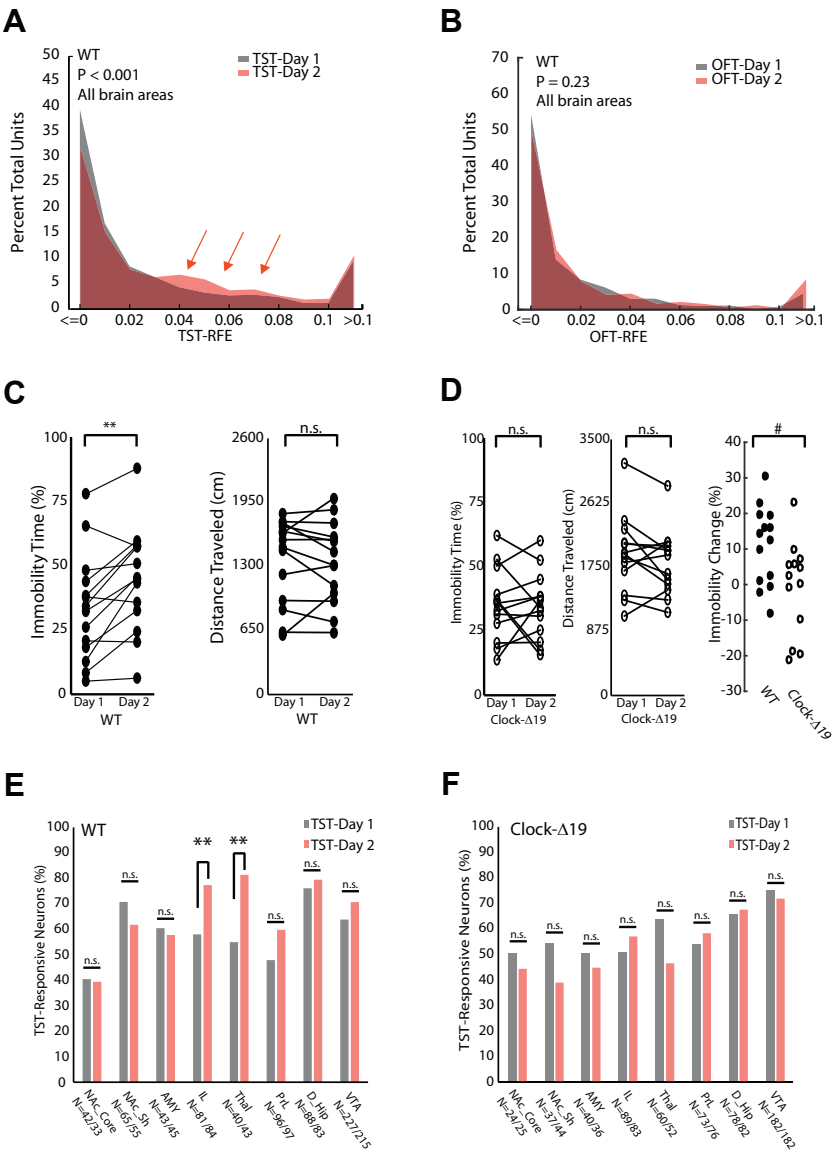

Figure 2. Infralimbic cortex and thalamic responses increase during repeat tail suspension test (TST) testing. Histograms of test-related neuronal firing for all neurons recorded during repeated **(A)** TST and **(B)** open field test (OFT) testing. Test-related firing was quantified using the reduction in fractional error (RFE) of our spike-behavioral models (*$p < .05$ for comparisons across days using Kolmogorov-Smirnov test; $n = 682$ and 655 units for day 1 and day 2, respectively). **(C)** Immobility time and distance traveled during repeat TST and OFT testing in wild-type (WT) mice (**$p < .01$ using paired t test; $n = 14$ for WT mice). **(D)** Immobility time and distance traveled during repeat TST and OFT testing in *Clock-Δ19* mice ($^{\#}p < .05$ for genotype × session effect of TST immobility using mixed-model analysis of variance; $n = 14$ WT mice and 13 mutant mice; $p > .05$ using paired t test for immobility time and distance travelled; $n = 13$ for *Clock-Δ19*). No statistical difference in the variance of the immobility change was observed across the two populations of mice (two-sample F test for equal variances [$F_{13,12} = 0.66$, $p = .47$]). **(E)** Area-specific expansion of TST-related movement function in WT mice (**$p < .05$ using G-test of independence with Williams correction). **(F)** No area-specific expansion of TST-related movement function was observed in *Clock-Δ19* mice ($p > .05$ for all comparisons using G-test of independence with Williams correction). AMY, amygdala; D_Hip, dorsal hippocampus; n.s., not significant; NAc_Core, nucleus accumbens core; NAc_Shell, nucleus accumbens shell; PrL, prelimbic cortex; Thal, medial dorsal thalamus; VTA, ventral tegmental area.

in the Thal (Figure 3A, B). Critically, CFPC between these structures increased across testing sessions (paired t test [$t_{13} = 3.3$, $p = .0059$]; Figure 3B), similar to the cellular and behavioral changes described above. The strength of IL-Thal CFPC exhibited by individual animals was directly related to their immobility time during both testing sessions ($p < .05$ for both comparisons using linear regression; Figure 3C), and this relationship became stronger during the second session (analysis of covariance [$F_{1,24} = 5.63$; $p = .026$]). Thus, the behavioral relevance of this circuit increased with repeated testing. Directionality analysis showed that 3-Hz to 7-Hz LFP activity in the IL temporally preceded oscillatory activity in the Thal, providing evidence that IL-Thal CFPC reflected directional activity in the IL-Thal pathway (Figure 3D). No differences in low-frequency (2–12 Hz) power within IL or Thal, or coherence between the two structures were observed across testing sessions ($F_{11,286} = 0.68$, 0.63, and 0.08; $p = .58$, .53, and .94, for comparison of cortical power, thalamic power, and IL-Thal coherence, respectively, using repeated measures ANOVA; Figure 3E). However, we found an increase in IL and Thal gamma power and coherence between across two testing sessions ($t_{13} = 5.68$, 3.53, and 4.28; $p = 7.5 \times 10^{-5}$, .004, and 9×10^{-4}, for comparison of cortical power, thalamic power, and IL-Thal coherence, respectively, using repeated measures ANOVA; Figure 3F). Thus, the adaptations in IL-Thal function that resulted from TST exposure were specific to the spatiotemporal dynamics involving gamma oscillatory across these brain areas.

After demonstrating that the IL and Thal cellular adaptations induced by stress were marked by changes in the spatiotemporal dynamics across IL-Thal circuitry, we set out to test whether the patterns we observed in IL-Thal circuitry were causally related to behavior. To accomplish this, we developed a new approach to manipulate spatiotemporal dynamics

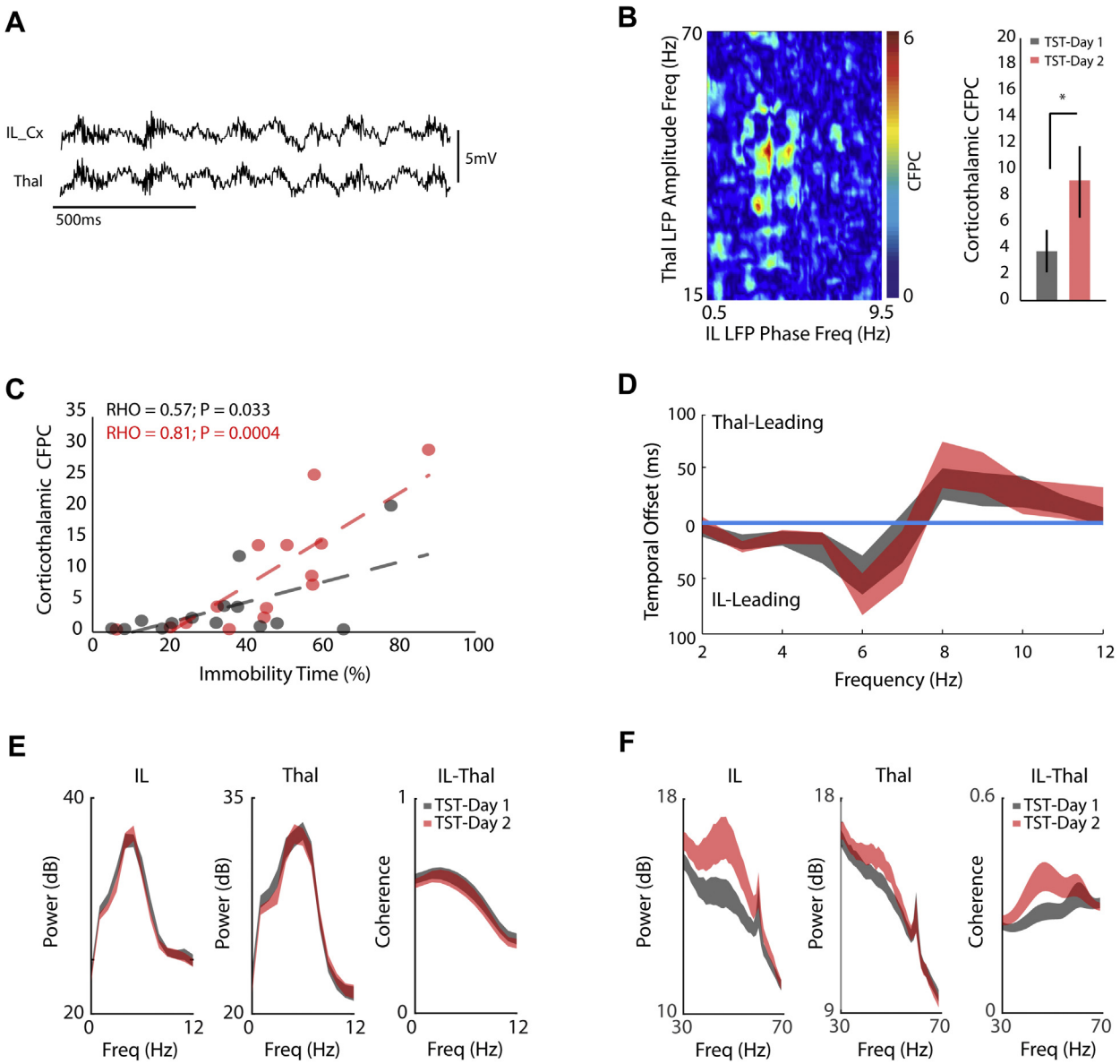

Figure 3. Limbic reorganization is specific to stress-induced behavioral adaptation. **(A)** Infralimbic cortex (IL_Cx) and medial dorsal thalamus (Thal) local field potential (LFP) traces (top). **(B)** Image shows coupling between the phase of IL oscillations in frequencies ranging from 0.5 to 9.5 Hz, and the amplitude of Thal oscillations ranging from 15 to 70 Hz (left). Cross-frequency phase coupling (CFPC) was quantified between IL 3–7-Hz oscillations and Thal 30–70-Hz oscillations across tail suspension test (TST) testing sessions ($p < .05$ using paired t test; $n = 14$ mice; right). **(C)** IL-Thal CFPC was directly correlated with the immobility time observed across animals ($p < .05$ using linear regression; bottom). This relationship increased across testing sessions ($p < .05$ using analysis of covariance). **(D)** Temporal offsets at which IL and Thal oscillations optimally phase synchronized at each frequency (figure shows 95% confidence interval observed across animals for both testing days; $n = 14$; top). Frequencies that showed significant lag did not overlap with zero offset. **(E)** IL and Thal 2–12 Hz power and IL-Thal 2–12 Hz coherence across testing sessions ($p > .05$ for all three measures across testing sessions using repeated measures analysis of variance; data shown as mean ± SEM). **(F)** IL and Thal gamma power and IL-Thal gamma coherence across testing sessions ($p < .05$ for all three measures across testing sessions using paired t test; data shown as mean ± SEM). Freq, frequency.

across prefrontal cortex (PFC)–dependent networks. Specifically, we injected a transsynaptic wheat germ agglutinin–tagged Cre recombinase (20) into the PFC (IL and prelimbic cortex) of mice naive to behavioral challenge. Infection with wheat germ agglutinin–tagged Cre recombinase results in high Cre expression in PFC neurons and modest Cre expression in the other neurons in the brain that form synaptic connections with PFC (both efferent and afferent synaptic connections). We then infected Thal with a floxed ultra-fast channelrhodopsin-2 variant (ChETA) (21) (Figure 4A; see also Supplemental Figure S5). This strategy ultimately resulted in ChETA expression in cortical neurons that projected to

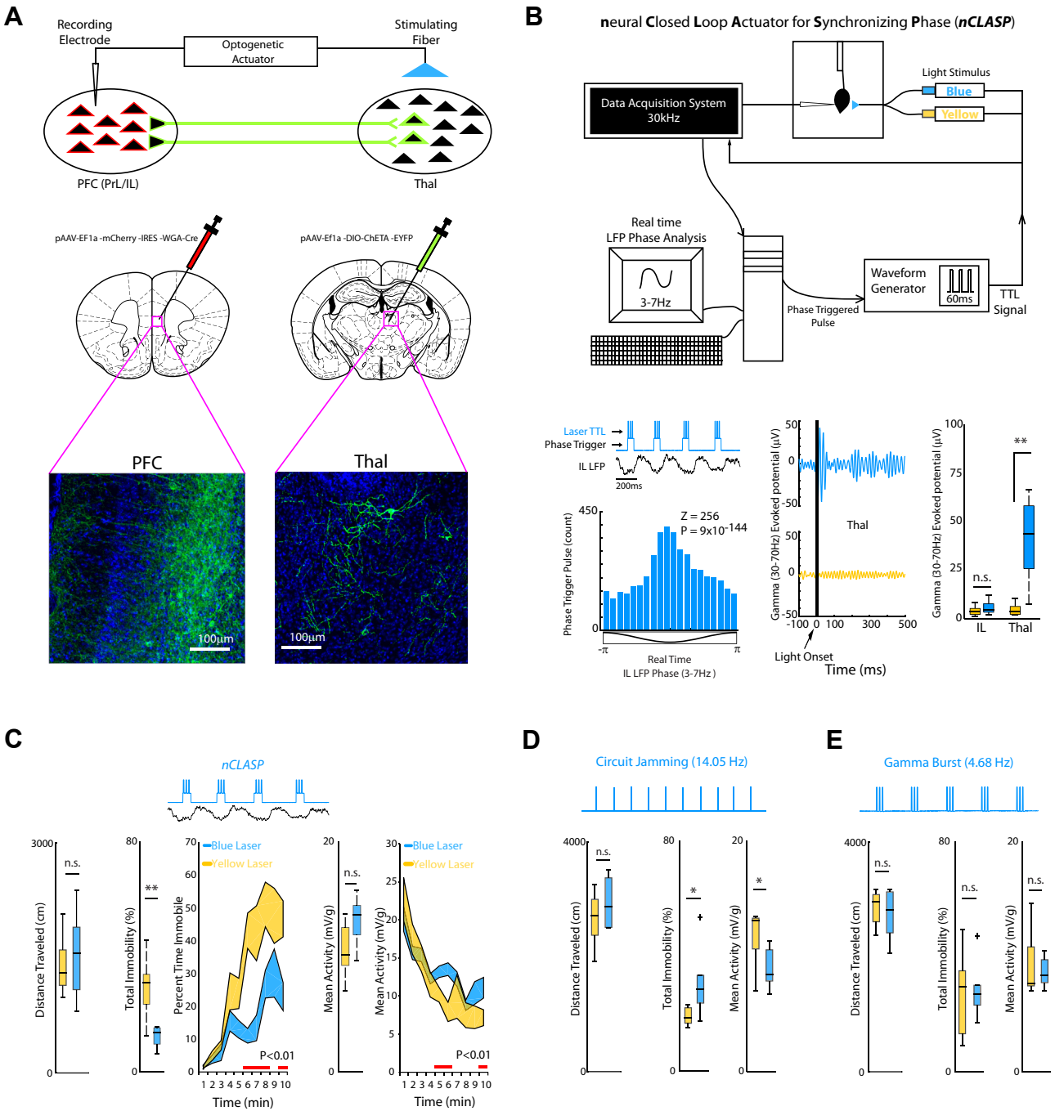

Figure 4. Properly timed infralimbic cortex (IL)–medial dorsal thalamus (Thal) stimulation increases resilience to behavioral challenge. **(A)** Schematic of protocol for IL-Thal stimulation (top), viral infection strategy (middle), and histological images (bottom). Enhanced yellow fluorescent protein (EYFP) expression was present in layer V/IV prefrontal cortex (PFC) neurons and their apical dendrites, PFC axon terminals in the Thal, and the soma of the Thal neurons (bottom). **(B)** Detailed schematic for *nCLASP* system (top). This protocol was used to deliver light pulses to Thal at the trough of IL 3–7-Hz oscillations (bottom). Histogram shows the IL phase distribution at which gamma pulses were initiated during a tail suspension test (TST) session. Phase coupling of gamma burst light pulses was quantified using the Rayleigh test where Z = –log(P) (bottom left). IL and Thal evoked activity during *nCLASP* stimulation. **(C)** Effects of *nCLASP* stimulation on open field test and TST behavior ($p < .01$ for comparison of blue and yellow light stimulation groups using repeated measures analysis of variance for TST behavior; red bars on the x axis highlight time points where $p < .05$ for post hoc testing using unpaired *t* test; data shown as mean ± SEM). Mean TST activity was quantified as millivolts per gram (mV/g) mouse. **(D, E)** Effects of two open-loop stimulation protocols on open field test and TST behavior (*$p < .05$, **$p < .01$ for comparison of total activity across groups using students *t* test; *n* = 6-8 mice/group). ChETA, floxed ultra-fast channelrhodopsin-2 variant; Cre, Cre recombinase; LFP, local field potential; n.s., not significant; PrL, prelimbic cortex; WGA, wheat germ agglutinin.

thalamus, thalamic neurons that received input from the PFC, and thalamic neurons that sent efferents to the PFC. Finally, we invented *nCLASP* to stimulate this subset of PFC axonal terminals and Thal neurons with gamma bursts timed to ongoing oscillatory activity in cortex (Figure 4B). *nCLASP* allowed us to drive bursts of Thal gamma activity that were phase-coupled to 3-Hz to 7-Hz oscillations in cortex, paralleling the CFPC physiological parameters of the IL-Thal circuit we measured during the TST. We calibrated this *nCLASP* system to deliver gamma bursts (three successive 5-ms light pulses with an interpulse interval of 15 ms) initiated at the rising phase of IL 3-Hz to 7-Hz oscillatory cycles (Figure 4B). Experimental animals were stimulated with blue light to activate ChETA and control animals were stimulated with yellow light, which does not activate the opsin (Figure 4B). Behavioral and neural responses were monitored while these animals were subjected to the TST. Stimulation with blue, but not yellow, light evoked Thal gamma activity (Figure 4B; unpaired *t* test [t_{13} = 1.2 and 4.8; p = .24 and .0003] for comparisons of IL- and Thal-evoked potential amplitude, respectively; n = 7–8 mice per group).

Activation of the IL-Thal circuit using *nCLASP* rendered the stress-naive mice more resilient to the behavioral adaptation that occurred within a TST session. Specifically, mice stimulated with blue light exhibited less immobility and higher activity profiles compared with the animals stimulated with yellow light (for light effect on immobility time [$F_{9,117}$ = 3.89, p = .008]; for light effect on mean activity [$F_{9,117}$ = 2.73, p = .009]; comparisons of blue and yellow light groups were made using repeated measures ANOVA; comparison of full test immobility time using Student's *t* test [t_{13} = 3.3, $p < .05$]; Figure 4C). Importantly, no differences in gross locomotion were observed when animals were stimulated in the open field (two-tailed Student's *t* test [t_{11} = –0.59; p = .57]), showing that stimulation of the IL-Thal pathway induced a behavioral effect that was specific to the TST paradigm. This was consistent with our findings that IL neurons preferentially signal behavior in the TST (compared with the OFT; see Figure 1D). Furthermore, IL-Thal stimulation had no impact on the immobility time or mean activity observed during the first 4 minutes of the TST (Figure 4C), demonstrating that this stimulation approach did not simply induce hyperactivity. Rather, stimulation of the IL-Thal pathway using *nCLASP* diminished the behavioral adaptation that occurred across the 10-minute TST session.

Next, we tested two additional open-loop patterns in a new group of stress-naive mice. Our first open-loop stimulation protocol was designed to deliver the same number of light pulses as *nCLASP*, but in a manner not linked to oscillatory activity in the cortex or local gamma oscillations (constant 14.05-Hz, 5-ms pulse width; see Figure 4D). IL-Thal stimulation with blue light reduced TST escape behavior during testing (two-tailed Student's *t* test [t_{10} = –2.24 and 2.27, p = .049 and 0.047] for full test immobility time and activity, respectively), though this stimulation had no impact on OFT behavior (two-tailed Student's *t* test [t_{10} = 1.5, p = .316]; see Figure 4D). Thus, IL-Thal circuit stimulation using *nCLASP* induced escape behaviors, while IL-Thal stimulation using open-loop stimulation at 14.05 Hz suppressed escape behaviors. Notably, the carrier frequency used for our first open-loop stimulation protocol was three times as fast as the carrier frequency of IL to Thal input (14.05 Hz compared with 2–7 Hz). Our second open-loop control stimulation was designed to deliver gamma bursts consisting of three light pulses at 4.68 Hz (14.05 Hz ÷ 3; see Figure 4E), which was similar to the frequency administered during *nCLASP* stimulation but, importantly, was not timed to IL activity. Stimulation with this open-loop pattern had no effect on TST behavior (two-tailed Student's *t* test [t_{10} = 0.13 and 0.45, p = .899 and 0.659] for full test immobility time and activity, respectively) or OFT behavior (Student's *t* test [t_9 = –0.57 and p = .582]; see Figure 4E). Thus, gamma burst stimulation of the IL-Thal pathway had to be timed to the endogenous IL oscillations to induce movement, and carrier stimulation frequencies above the normal input frequency of the pathway (2–7Hz) suppressed it.

DISCUSSION

The TST is widely used as a preclinical model of MDD due to the assay's sensitivity to acute treatment with clinically relevant antidepressants. Additional testing is typically performed in an open field to clarify whether pharmacological/genetics manipulations induce TST activity due to their specific antidepressant-like effects or because they more generally induce hyperactivity. The TST is classically performed during a single 6-minute session in mice (7). However, to exploit the observation that the TST induces a robust stress response (9), we performed neural recordings during two TST sessions on successive days. This approach allowed us to concurrently dissect both the neural circuits responsible for TST escape action under normal conditions and the behaviorally relevant neural adaptions induced by repeated stress exposure.

Using a linear decoder, we found that neurons in all the cortical and limbic regions we probed exhibited firing linked to TST movement. Furthermore, many cells in these areas signaled movement in the TST but not in the OFT. Thus, either a different set of movements were induced by the two tests or a different population of cells encoded the overlapping set of movements induced by the two distinct tests. In both instances, the cellular responses we discovered clearly demonstrate that the OFT and TST exploit distinct neural processes reflected across limbic circuitry. The differential sensitivity of TST and OFT-related movement to acute antidepressant treatment may be due to these nonoverlapping neuronal responses. Importantly, while immobility during the TST by no means recapitulates the range of symptoms observed across MDD (22), our findings suggest that the TST can indeed be used to effectively probe the function of widely distributed brain networks implicated in MDD. Normal TST behavior reflects normal function in these brain networks, and altered activity in the brain areas that compose the TST network can be reflected by behavioral dysfunction in the TST versus the OFT. Additional experiments will be needed to clarify the exact nature of the information that is encoded by these TST movement–related neurons.

Repeated TST-stress exposure selectively induced changes in IL and Thal firing. Based on the spatiotemporal dynamics observed between IL and Thal, our findings showed that IL-Thal CFPC was directly correlated with TST immobility during the initial testing session. Paradoxically, the correlation slope between IL-Thal CFPC and TST immobility increased

during the repeat TST session (see Figure 3C), such that the amount of immobility exhibited by mice during the second session was lower than expected based on their IL-Thal CFPC. Consistent with the observations that direct PFC stimulation induces an antidepressant-like effect in multiple MDD-related test paradigms (6,23), these findings suggested that IL-Thal CFPC may reflect a neurophysiological process that induces TST movement. When we used our *nCLASP* system to recapitulate the spatiotemporal dynamic we identified in IL-Thal circuitry, our findings confirmed that IL-Thal CFPC induces TST-related movement. Importantly, though we found that gamma power increased across the IL-Thal circuit with repeat TST exposure, open-loop gamma stimulation of the circuit had no behavioral effect. Taken together, these results indicate that IL-Thal CFPC likely reflects a compensatory circuit (i.e., circuit adaptations that occur in an attempt to return neural systems to homeostasis). This circuit is activated in response to uncontrollable stress, and disruption of the spatiotemporal dynamic observed in this circuit using an open-loop stimulation above the circuit carrier frequency (circuit jamming) renders animals less tolerant to stress. Critically, additional experiments will be needed to dissect the primary circuit changes that promote increases in TST immobility in response to stress.

It remains unknown whether the IL-Thal compensatory circuit we found diminishes the subjective stress experience or activates behavior that counters the behavioral stress response; nevertheless, it holds promise as a target for further research into its therapeutic potential. For example, the spatiotemporal dynamic patterns we identified in the IL-Thal circuit may serve as a preclinical biomarker of stress-induced behavioral dysfunction that can be exploited for therapeutic development. Future experiments that probe the impact of antidepressant treatment on IL-Thal CFPC are warranted. These experiments may also prove useful in dissecting the primary circuit adaptations that result from stress exposure.

Conclusions

Overall our *nCLASP* stimulation system induced escape behaviors in naive mice during the TST, while stimulation using a standard open-loop protocol that delivered an equivalent number of light pulses with a different carrier frequency tended to have the opposing effect (circuit jamming). This finding provides clear evidence that the neural state timing at which stimulation is delivered plays a critical role in determining the impact of cellular activation on behavior. This principle has particularly profound implications for interpreting the link between the activity of specific cell types and behavior, and for optimizing deep brain stimulation–based therapies. Critically, these findings also raise the provocative hypothesis that stress-induced behavioral disorders may result from altered neural timing across widely distributed circuits.

ACKNOWLEDGMENTS AND DISCLOSURES

This work was supported by an International Mental Health Research Organization/One Mind Rising Star Award, National Institute of Mental Health Grant No. R01MH099192, a generous contribution from Kerima L. Collier (to KD), and National Science Foundation Grant No. DGF1106401 (to M-ATV).

DC modeled spike-behavioral activity relationships, and analyzed neuronal data; LKD performed viral surgeries, and optogenetic stimulation experiments; NMG jointly developed methods for closed loop optogenetic stimulation with KD; M-ATV jointly conceived analytical methods for local field potential analysis, interpreted data, and wrote the paper with KD; MS integrated and synchronized the TST apparatus with neurophysiological recording system, and analyzed continuous TST behavioral measurements; CB scored TST behavioral activity from video recordings. RH performed ChR2 histological confirmations and helped to write the paper; JW constructed recording and stimulation electrodes, performed implantation surgeries, and assistant with ChR2 histological confirmations; CAM provided mice and helped to write the paper; LC provided oversight for spike-behavioral activity modeling and analysis; SK performed implantation surgeries and behavioral experiments for in vivo recording TST studies, and confirmed implantation sites histologically; SDM performed viral and electrode surgeries with LKD for optogenetic stimulation experiments, and performed ChR2 histological confirmations; KD conceived in vivo TST and optogenetic experiments, analyzed spike-behavioral activity data, performed local field potential analysis, developed closed-loop stimulation methods with NMG, and wrote the paper with M-ATV, with input from LKD, DC, RH, CAM, LC, and SDM.

We would like to thank K. Deisseroth for generously proving access to viral tools; L. Jiang-Xie and F. Wang for generating the ChR2 confocal microscopy image; and H. Mayberg, M. M. Halassa, I. Chou, and S. Lisberger for helpful comments on this manuscript. We also give special thanks to Freeman Hrabowski, Robert and Jane Meyerhoff, and the Meyerhoff Scholarship Program.

The authors report no biomedical financial interests or potential conflicts of interest.

ARTICLE INFORMATION

From the Department of Electrical and Computer Engineering (DC, LC), Duke University; and Department of Psychiatry and Behavioral Sciences (LKD, RH, JW, CB, SK, SDM, KD), Department of Biomedical Engineering (NMG, KD), Department of Neurobiology (NMG, M-ATV, KD), Center for Neuroengineering (KD), Duke Institute for Brain Sciences (LC, KD), Duke University Medical Center, Durham, North Carolina; Department of Statistics and Grossman Center for the Statistics of Mind (DC), Columbia University, New York, New York; Meyerhoff Scholarship Program (MS), University of Maryland, Baltimore County, Baltimore Maryland; and the Department of Psychiatry (CAM), University of Pittsburgh Medical School, Pittsburgh, Pennsylvania.

DC, LKD, NMG, and M-ATV contributed equally to this work.

Address correspondence to Kafui Dzirasa, M.D., Ph.D., Department of Psychiatry and Behavioral Sciences, Duke University Medical Center, 361 Bryan Research Building, Box 3209, Durham, NC 27710; E-mail: kafui.dzirasa@duke.edu.

Received Jan 3, 2017; revised May 31, 2017; accepted Jun 1, 2017.

Supplementary material cited in this article is available online at http://dx.doi.org/10.1016/j.biopsych.2017.06.008.

REFERENCES

1. Drevets WC, Price JL, Simpson JR Jr, Todd RD, Reich T, Vannier M, *et al.* (1997): Subgenual prefrontal cortex abnormalities in mood disorders. Nature 386:824–827.
2. Mayberg HS, Liotti M, Brannan SK, McGinnis S, Mahurin RK, Jerabek PA, *et al.* (1999): Reciprocal limbic-cortical function and negative mood: converging PET findings in depression and normal sadness. Am J Psychiatry 156:675–682.
3. Sheline YI, Price JL, Yan Z, Mintun MA (2010): Resting-state functional MRI in depression unmasks increased connectivity between networks via the dorsal nexus. Proc Natl Acad Sci U S A 107:11020–11025.
4. Mayberg HS, Lozano AM, Voon V, McNeely HE, Seminowicz D, Hamani C, *et al.* (2005): Deep brain stimulation for treatment-resistant depression. Neuron 45:651–660.
5. Fox MD, Buckner RL, White MP, Greicius MD, Pascual-Leone A (2012): Efficacy of transcranial magnetic stimulation targets for depression is related to intrinsic functional connectivity with the subgenual cingulate. Biol Psychiatry 72:595–603.

6. Hamani C, Diwan M, Macedo CE, Brandao ML, Shumake J, Gonzalez-Lima F, *et al.* (2010): Antidepressant-like effects of medial prefrontal cortex deep brain stimulation in rats. Biol Psychiatry 67:117–124.
7. Steru L, Chermat R, Thierry B, Simon P (1985): The tail suspension test: a new method for screening antidepressants in mice. Psychopharmacology (Berl) 85:367–370.
8. Tye KM, Mirzabekov JJ, Warden MR, Ferenczi EA, Tsai HC, Finkelstein J, *et al.* (2013): Dopamine neurons modulate neural encoding and expression of depression-related behaviour. Nature 493:537–541.
9. Ide S, Sora I, Ikeda K, Minami M, Uhl GR, Ishihara K (2010): Reduced emotional and corticosterone responses to stress in mu-opioid receptor knockout mice. Neuropharmacology 58:241–247.
10. Iniguez SD, Aubry A, Riggs LM, Alipio JB, Zanca RM, Flores-Ramirez FJ, *et al.* (2016): Social defeat stress induces depression-like behavior and alters spine morphology in the hippocampus of adolescent male C57BL/6 mice. Neurobiol Stress 5:54–64.
11. King DP, Zhao Y, Sangoram AM, Wilsbacher LD, Tanaka M, Antoch MP, *et al.* (1997): Positional cloning of the mouse circadian clock gene. Cell 89:641–653.
12. Carlson D, Schaich Borg J, Dzirasa K, Carin L (2014): On the relations of LFPs & neural spike trains. In: Gharamani Z, Welling M, Cortes C, Lawrence ND, Weinberger KQ, editors. Advances in Neural Information Processing Systems 27 (NIPS 2014). Available at: https://papers.nips.cc/paper/5404-on-the-relations-of-lfps-neural-spike-trains.pdf Accessed July 7, 2017.
13. Warden MR, Selimbeyoglu A, Mirzabekov JJ, Lo M, Thompson KR, Kim SY, *et al.* (2012): A prefrontal cortex-brainstem neuronal projection that controls response to behavioural challenge. Nature 492:428–432.
14. Roybal K, Theobold D, Graham A, DiNieri JA, Russo SJ, Krishnan V, *et al.* (2007): Mania-like behavior induced by disruption of CLOCK. Proc Natl Acad Sci U S A 104:6406–6411.
15. Dzirasa K, McGarity DL, Bhattacharya A, Kumar S, Takahashi JS, Dunson D, *et al.* (2011): Impaired limbic gamma oscillatory synchrony during anxiety-related behavior in a genetic mouse model of bipolar mania. J Neurosci 31:6449–6456.
16. Sidor MM, Spencer SM, Dzirasa K, Parekh PK, Tye KM, Warden MR, *et al.* (2015): Daytime spikes in dopaminergic activity drive rapid mood-cycling in mice. Mol Psychiatry 20:1406–1419.
17. Likhtik E, Stujenske JM, Topiwala MA, Harris AZ, Gordon JA (2014): Prefrontal entrainment of amygdala activity signals safety in learned fear and innate anxiety. Nat Neurosci 17:106–113.
18. Dzirasa K, Ramsey AJ, Takahashi DY, Stapleton J, Potes JM, Williams JK, *et al.* (2009): Hyperdopaminergia and NMDA receptor hypofunction disrupt neural phase signaling. J Neurosci 29:8215–8224.
19. Dzirasa K, Coque L, Sidor MM, Kumar S, Dancy EA, Takahashi JS, *et al.* (2010): Lithium ameliorates nucleus accumbens phase signaling dysfunction in a genetic mouse model of mania. J Neurosci 30:16314–16323.
20. Gradinaru V, Zhang F, Ramakrishnan C, Mattis J, Prakash R, Diester I, *et al.* (2010): Molecular and cellular approaches for diversifying and extending optogenetics. Cell 141:154–165.
21. Gunaydin LA, Yizhar O, Berndt A, Sohal VS, Deisseroth K, Hegemann P (2010): Ultrafast optogenetic control. Nat Neurosci 13:387–392.
22. Nestler EJ, Hyman SE (2010): Animal models of neuropsychiatric disorders. Nat Neurosci 13:1161–1169.
23. Hultman R, Mague SD, Li Q, Katz BM, Michel N, Lin L, *et al.* (2016): Dysregulation of prefrontal cortex-mediated slow-evolving limbic dynamics drives stress-induced emotional pathology. Neuron 91:439–452.